Investigation and modelling of the microstructure evolution during hot deformation of novel Fe–30Mn–10Al–3Si–1C with an elevated specific strength

A. A. Kazakova, *Master Student, Dept. of Physical Metallurgy of Non-ferrous Metals* [1];
A. V. Pozdnyakov, *Ph. D., Associate Prof., Dept. of Physical Metallurgy of Non-ferrous Metals* [1];
V. V. Cheverikin, *Ph. D., Leading Researcher, Dept. of Physical Metallurgy of Non-ferrous Metals* [1];
A. Yu. Churyumov, *Ph. D., Associate Prof., Dept. of Physical Metallurgy of Non-ferrous Metals* [1],
e-mail: churyumov@misis.ru

[1] *National University of Science and Technology "MISIS" (Moscow, Russia)*

The development of steel with high specific strength is required for reducing vehicles' weight and decrease of carbon dioxide emissions and fuel consumption. The most promising direction is the development of steels containing light elements such as manganese, aluminum, silicon, additionally alloyed with carbon. The final mechanical properties of these steels are affected by hot plastic deformation, which transforms the cast microstructure into a fine-grain one. Fe–30Mn–10Al–3Si–1C steel in the cast state was studied in this work. Compression tests were carried out in the range of strain rates of 0.1, 1, and 10 s^{-1} and temperatures of 900–1100 °C on the Gleeble 3800 thermomechanical simulator. The models of the relationship of flow stress and grain size with hot plastic deformation parameters were constructed. These models can be used to develop and optimize technologies for hot plastic deformation of Fe–30Mn–10Al–3Si–1C steel. The studied steel has a high level of hardness after hot deformation in the temperature range of 1000–1050 °C due to the formation of a fine grain microstructure, which can guarantee a high specific strength of the final products obtained using optimized hot plastic deformation modes.

Key words: Fe–Mn–Al–C steel, hot deformation, modeling, microstructure, flow stress, thermomechanical simulator Gleeble.
DOI: 10.17580/cisisr.2024.01.10

Introduction

High-manganese steels are promising materials for the automotive industry due to their increased specific strength and low cost. Such materials have a high strength, ductility, and impact strength at room temperature [1–6]. In addition, they show high energy absorption under impact loads, which can have a significant impact during traffic accidents [7, 8]. The properties of steel are determined by the chemical composition and production technology, including high-temperature deformation [9, 10]. In this regard, the behavior of these alloys under hot deformation conditions requires a detailed study.

The alloys of the Fe–Mn–Al–C system can be divided into 4 categories: ferritic, ferrite-based duplex, austenite-based duplex, and austenitic steels. The increase in specific strength in these alloys occurs due to a decrease in the average atomic mass and dilatation of the crystal lattice.

Austenitic steels usually contain 12–30 % of manganese, 5–12 % of aluminum, and 0.6–2 % of carbon. Manganese is an austenite stabilizer, however, when more than 6 % Al is added to steels with 30 % Mn, the steel ceases to be austenitic, and δ-ferrite appears [11]. Carbon is an excellent stabilizer of austenite, therefore, the addition of 1 % C by weight in Fe–9Al–30Mn can make steel completely austenitic, but with a decrease in the carbon content, a ferritic phase appears [12].

Alloying by Al reduces steel's density and stiffness, as well as increases the stacking-fault energy providing the dislocation mechanism of deformation. Dislocation sliding occurs by waves, the mechanism of transverse dislocation sliding is activated and dislocation walls are formed [13]. The addition of more than 3% aluminum contributes to the appearance of spinodal decomposition during the quenching process, due to which, first the short-range order $L1_2$ is formed, then coherent with the austenitic matrix carbides with the structural type $E2_1$ (perovskite) of the chemical formula $(Fe, Mn)_3AlC_x$, where $x < 1$ are released.

The formation of $(Fe, Mn)_3AlC_x$ occurs both in the grain body (κ'-carbides) and along the grain boundaries (κ-carbides). After prolonged aging, austenite begins to decompose into ferrite and κ-carbides or ferrite, κ-carbides, and β-Mn [14].

The addition of a small amount (1–3 %) of Si improves the casting properties of steel and increases the yield strength by accelerating the kinetics of the formation of κ-carbides in the grain body and their stabilization at high temperatures. However, further addition of silicon increases the probability of formation of κ-carbides at the grain boundary, which leads to a deterioration of the mechanical properties [15, 16]. Also, when silicon is added, an oxide layer $(Fe, Mn)_2SiO_4$ is formed on the surface, which increases the corrosion resistance of steel.

Hot deformation is a necessary part of the full production cycle of most metal semi-finished products; therefore, much attention has recently been paid to the study of this process in steels of the Fe–Mn–Al–C system [17–20]. The grain microstructure that formed during hot working has a significant effect on the final mechanical properties. In this regard, simulation of the process of hot deformation allows for optimizing the technology of metal forming, including using the widely used finite element method [21–24].

The purpose of this work is the investigation and construction of mathematical models for the evolution of the microstructure of novel Fe–30Mn–10Al–3Si–1C steel with increased specific strength under hot plastic deformation.

Materials and methods

Steel with the nominal composition Fe–30Mn–10Al–3Si –1C was chosen as the object of the study. Ingots with a diameter of 6 and a length of 60 mm were obtained from row materials of technical purity by induction melting in argon using an Indutherm 20V furnace. Casting was carried out to a copper mold under the pressure of 3 atm. Samples for hot deformation had a radius of 3 mm and a height of 9 mm. Compression to the true strain of 1 was carried out on a Gleeble 3800 thermomechanical simulator at temperatures of 900–1100 °C and strain rates of 0.1, 1, and 10 s^{-1}. The obtained primary stress-strain curves were corrected taking into account the friction between the dies and the edges of the sample, as well as taking into account the adiabatic heating during compression according to the earlier developed method [25].

A Carl Zeiss Axiovert light microscope, a Tescan-VEGA3LMH scanning electron microscope was used for the microstructural analysis. Metallographic samples were obtained by polishing using Struers LaboPol-5. The linear intercept method was used to determine the average grain size. Five images were analyzed for each state, and the average number of measurements was about 100. Microhardness was determined using Wolpert 402 MVD hardness tester with a load of 100 g.

Results and discussion

Fig. 1 shows the image of the Fe–30Mn–10Al–3Si–1C steel microstructure in the as-cast state. Mainly two phases are presented in the steel's microstructure: ferrite (yellow color) with the following chemical composition Fe–24Mn–12Al–3.7Si and a volume fraction of 21.2 % and austenite (blue color) with the following chemical composition Fe–32Mn–9Al–4, 2Si–1.6C and a volume fraction of 78.8 %. In addition, a phase with an increased manganese content and a reduced aluminum concentration (Fe–39Mn–9Al–4.2Si–1.6C) (white particles in Fig. 1a) were present in the microstructure.

An analysis of the compression curves at elevated temperatures (**Fig. 2**) showed that the flow stress decreases with increasing temperature and decreasing strain rate. Besides, all compression curves exhibit a maximum at the initial stage of deformation, which corresponds to the onset of intense dynamic recrystallization processes, leading to a significant decrease in the flow stress due to a reduction in the average dislocation density.

The Ziner-Hollomon parameter (Z) was used for the description of the relationship between flow stress, strain rate, and temperature:

$$Z = \dot{\varepsilon} e^{\frac{Q}{RT}} \quad (1)$$

where $\dot{\varepsilon}$ is a strain rate (s^{-1}), T is a temperature (K), Q is an effective activation energy of deformation (J/mole), and R is the universal gas constant (8.314 J/moleK). It is known that under the different deformation conditions the relation between Z and flow stress may be described by a power law (*2*), exponential law (*3*), and hyperbolic sine law (*4*):

$$Z = A_1 \sigma^{n_1} \quad \text{(for low } \sigma\text{)} \quad (2)$$

$$Z = A_2 e^{\beta\sigma} \quad \text{(for high } \sigma\text{)} \quad (3)$$

$$Z = A_3 [sinh(\alpha\sigma)]^{n_2} \quad \text{(for } \sigma \text{ values over a wide range)} \quad (4)$$

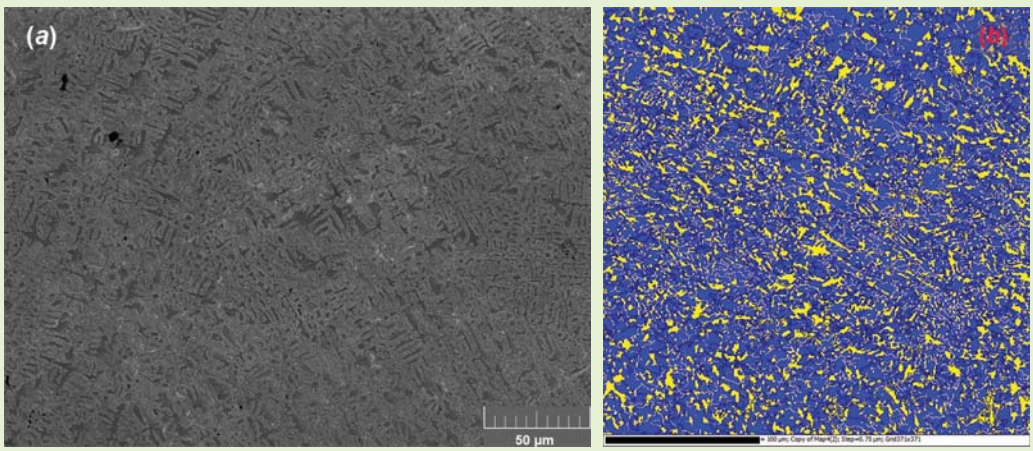

Fig. 1. Microstructure of Fe–30Mn–10Al–3Si–1C steel in the as-cast state: image in backscattered electrons *(a)*, phase distribution obtained by electron backscattered diffraction *(b)*

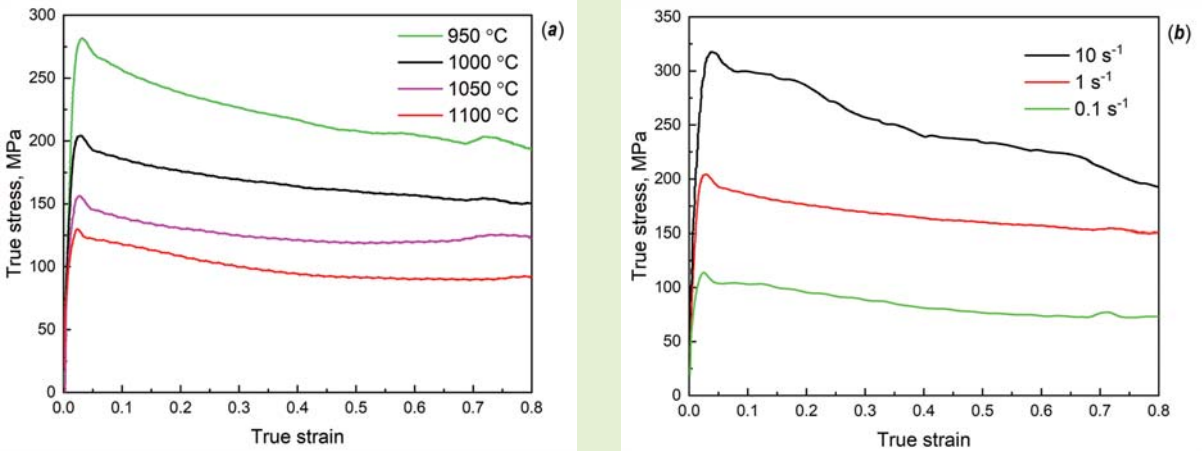

Fig. 2. Compression curves of Fe–30Mn–10Al–3Si–1C steel at the strain rate of 1 s^{-1} (a) and the temperature of 1000 °C (*b*)

where A_1, A_2, A_3, n_1, n_2, β, and α are the material constants. The value of the coefficient α is related to the constants n_1 and β by the following equation:

$$\alpha \approx \frac{\beta}{n_1} \quad (5)$$

The values of the unknown constants were determined by the least-squares method using the values of the peak flow stress. As a result, the quantified dependence accordingly equation (4) is following:

$$\dot{\varepsilon} e^{\frac{330000}{RT}} = 2 \cdot 10^{13} [sinh(0.0047\sigma)]^{3.65} \quad (6)$$

A comparison of the calculated and experimental values of flow stress shows that the average calculation error was 2.8 %. The value of effective activation energy for hot plastic deformation was 330 kJ/mol, which is significantly lower than the value of silicon-free high Mn steels (385 kJ/mol for Fe–28Mn–8Al–1C steel [26], 432 kJ/mol for Fe–35Mn–10Al–1C steel [27]), which may indicate the facilitation of the deformation process due to accelerated dynamic recovery and recrystallization.

The microstructure of the steel after the hot deformation is shown in **Fig. 3**. It can be seen that dynamic recrystallization and grain growth take place at an elevated temperature. At temperatures below 1000 °C, the structure contains

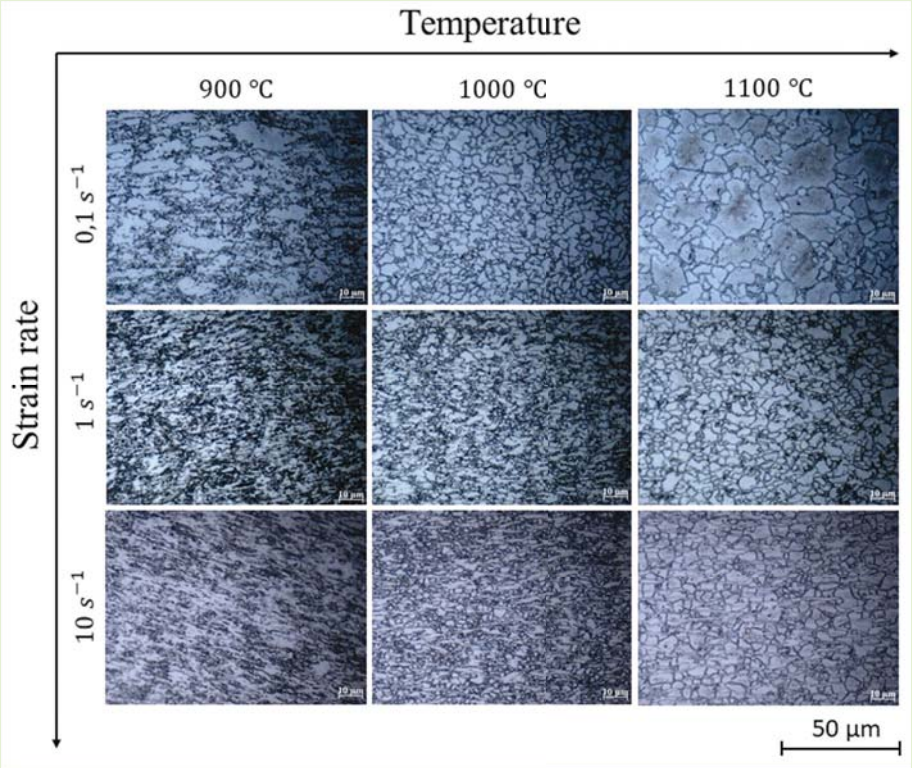

Fig. 3. Microstructure of Fe–30Mn–10Al–3Si–1C steel after hot plastic deformation

elongated non-recrystallized grains and areas along their boundaries with small grains formed during dynamic recrystallization.

The average grain size was measured in the samples where dynamic recrystallization fully proceeded. The obtained values were used to construct a mathematical model for the prediction of dynamically recrystallized grain size under different temperatures and strain rates:

$$d = 64500 \cdot \dot{\varepsilon}^{-0.128} \cdot exp\left(\frac{-108700}{RT}\right) \quad (7)$$

Fig. 4 shows the calculated dependence of the dynamically recrystallized grain size on temperature and strain rate. The points corresponding to the experimental values of the grain size are plotted on the graph. The average error was 22 %.

The studied steel has a high hardness in the cast state (HV500 ± 4). This high level is also preserved after the hot deformation. The dependence of microhardness on the modes of thermal deformation treatment is shown in **Fig. 5**. The decrease in microhardness with the deformation temperature is associated with the occurrence of softening processes such as dynamic recovery and recrystallization. However, at a temperature of 950 °C, a minimum is observed, apparently associated with a change in the phase composition at a given temperature. An increase in the mass fraction of ferrite with an increased stacking fault energy leads to an acceleration of the dynamic recovery process and, as a consequence, a significant decrease in the dislocation density, which affects the overall level of strength after the deformation at a given temperature.

Conclusions

1. The microstructure and microhardness of Fe–30Mn–10Al–3Si–1C steel in the as-cast and hot-deformed states were studied. It is shown that during the deformation in the temperature range of 1000–1050 °C, a completely recrystallized structure with a grain size of 3–8 μm is formed, which contributes to high microhardness values of HV500–600.

2. A mathematical model of the relationship between the flow stress and the parameters of hot plastic deformation has been constructed. It is shown that doping with silicon leads to a significant decrease in the value of the effective activation energy.

3. A model for the relationship between the size of dynamically recrystallized grains and temperature and strain rate was built. The constructed model can be used to predict the microstructure and optimize hot plastic deformation technologies.

This research was funded by the Russian Science Foundation (project №18-79-10153-P).

REFERENCES

1. Chen S., Rana R., Haldar A., Ray R. K. Current state of Fe–Mn–Al–C low density steels. *Progress in Materials Science*. 2017. Vol. 89. pp. 345–391.
2. Mishra B., Sarkar R., Singh V., Kumar D., Mukhopadhyay A., Madhu V., Prasad M. J. N. V. Effect of Cold Rolling and Subsequent Heat Treatment on Microstructural Evolution and Mechanical Properties of Fe–Mn–Al–C–(Ni) Based Austenitic Low-Density Steels. *SSRN Electronic Journal*. 2022. Vol. 861.
3. Jeong S., Park G., Kim B., Moon J., Park S. J., Lee C. Precipitation behavior and its effect on mechanical properties in weld heat-affected zone in age hardened Fe–Mn–Al–C lightweight steels. *Materials Science and Engineering A*. 2019. Vol. 742. pp. 61–68.
4. Ren P., Chen X. P., Yang M. J., Liu S. M., Cao W. Q. Effect of early stage of κ-carbides precipitation on tensile properties and deformation mechanism in high Mn–Al–C austenitic low-density steel. *Materials Science and Engineering A*. 2022. Vol. 857. p. 144132.
5. Svyazhin A. G., Bazhenov V. E., Kaputkina L. M., Smarygina I. V, Kindop V. E. Nitrogen In Fe–Mn–Al–C – based steels. *CIS Iron and Steel Review*. 2016. Vol. 12. pp. 13–17.

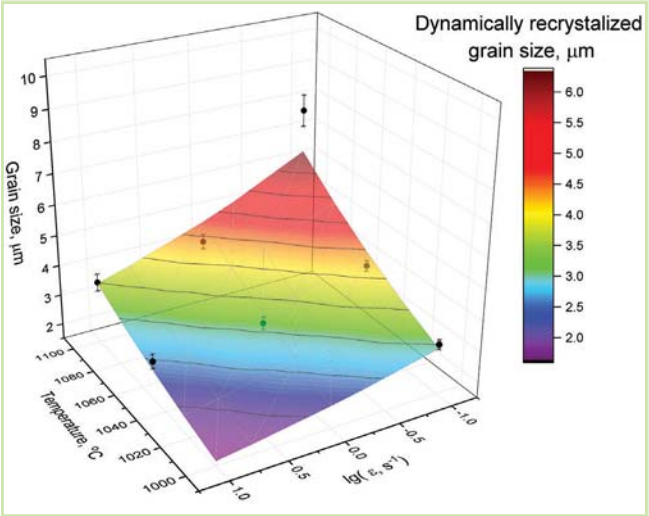

Fig. 4. Dependence of the dynamically recrystallized grain size on the parameters of the hot deformation (surface is a prediction, dots are experimental values)

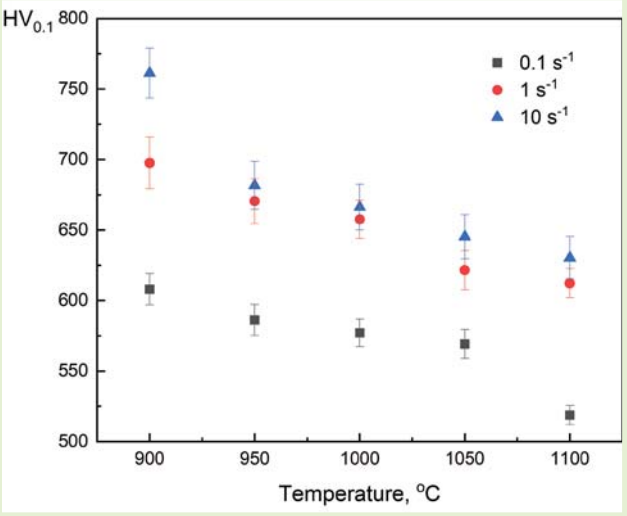

Fig. 5. Microhardness of Fe–30Mn–10Al–3Si–1C steel after the hot plastic deformation

6. Arapov S. L., Belyaev S. V., Kosovich A. A., Partyko E. G. Digital experiment as a method for improving the mechanical properties of Hadfield steel. *Chernye Metally*. 2022. No. 10. pp. 45–51.
7. Jabłońska M. B., Kowalczyk K. Microstructural aspects of energy absorption of high manganese steels. *Procedia Manufacturing*. 2019. Vol. 27. pp. 91–97.
8. Efremov D. B., Gerasimova A. A., Gorbatyuk S. M., Chichenev N. A. Study of kinematics of elastic-plastic deformation for hollow steel shapes used in energy absorption devices. *CIS Iron and Steel Review*. 2019. Vol. 18. pp. 30–34.
9. Rauch L., Madej L., Spytkowski P., Golab R. Development of the cellular automata framework dedicated for metallic materials microstructure evolution models. *Archives of Civil and Mechanical Engineering*. 2015. Vol. 15. pp. 48–61.
10. Mozumder Y. H., Arun Babu K., Saha R., Mandal S. Flow characteristics and hot workability studies of a Ni-containing Fe–Mn–Al–C lightweight duplex steel. *Materials Characterization*. 2018. Vol. 146. pp. 1–14.
11. Frommeyer G., Brüx U. Microstructures and Mechanical Properties of High-Strength Fe–Mn–Al–C Light-Weight TRIPLEX Steels. *Steel research international*. 2006. Vol. 77. pp. 627–633.
12. Tjong S.C. Electron Microscope Observations of Phase Decompositions in an Austenitic Fe–8.7AI–29.7Mn–1.04C Alloy. *Materials Characterization*. 1990. Vol. 24. pp. 275–292.
13. Bay B., Hansen N., Hughes D. A., Kuhlmann-Wilsdorf D. Evolution of f.c.c. deformation structures in polyslip. *Acta Metallurgica Et Materialia*. 1992. Vol. 40. pp. 205–219.
14. Lee J. W., Liu T. F. Phase transformations in an Fe–8Al–30Mn–1.5Si–1.5C alloy. *Materials Chemistry and Physic*s. 2001. Vol. 69. pp. 192–198.
15. Ren X., Li Y., Qi Y., Wang C. Effect of Micro-Alloyed/Alloyed Elements on Microstructure and Properties of Fe–Mn–Al–C *Lightweight Steel. Metals*. 2022. Vol. 12. No. 695.
16. Kim C. W., Terner M., Lee J. H., Hong H. U., Moon J., Park S. J., Jang J. H., Lee C. H., Lee B. H., Lee Y. J. Partitioning of C into κ-carbides by Si addition and its effect on the initial deformation mechanism of Fe–Mn–Al–C lightweight steels. *Journal of Alloys and Compounds*. 2019. Vol. 775. pp. 554–564.
17. Yang F. Q., Song R. B., Zhang L. F., Zhao C. Hot deformation behavior of Fe–Mn–Al light-weight steel. *Procedia Engineering*. 2014. Vol. 81. pp. 456–461.
18. Wan P., Yu H., Li F., Gao P., Zhang L., Zhao Z. Hot Deformation Behaviors and Process Parameters Optimization of Low-Density High-Strength Fe–Mn–Al–C Alloy Steel. *Metals and Materials International*. 2022. Vol. 28. pp. 2498–2512.
19. Shen Y., Liu J., Xu H., Liu H. High-Temperature Tensile Properties and Deformation Behavior of Three As-Cast High-Manganese Steels. *Steel Research International*. 2021. Vol. 92. pp. 1–12.
20. Renault C., Churyumov A. Y., Pozdniakov A. V., Churyumova T. A. Microstructure and hot deformation behavior of Fe–Mn–Al–C–Mo steel. *Journal of Materials Research and Technology*. 2020. Vol. 9. pp. 4440–4449.
21. Gorbunova Y. D., Orlov G. A. Simulation of hot stamping of elliptical steel bottoms. *Chernye Metally*. 2019. No. 10. pp. 58–62.
22. Churyumov A. Y., Medvedeva S. V., Mamzurina O. I., Kazakova A. A., Churyumova T. A. United Approach to Modelling of the Hot Deformation Behavior, Fracture, and Microstructure Evolution of Austenitic Stainless AISI 316Ti Steel. *Applied Sciences*. 2021. Vol. 11. No. 3204.
23. Lisunets N. L. Improving the efficiency of the processes of billets manufacture from rolled metal via shift cutting based on simulation. *Chernye Metally*. 2018. No. 6 pp. 31–35.
24. Zhong L., Wang B., Hu C., Zhang J., Yao Y. Hot deformation behavior and dynamic recrystallization of ultra high strength steel. *Metals*. 2021. Vol. 11. No. 1239.
25. Churyumov A. Y., Khomutov M. G., Tsarkov A. A., Pozdnyakov A. V., Solonin A. N., Efimov V. M., Mukhanov E. L. Study of the structure and mechanical properties of corrosion-resistant steel with a high concentration of boron at elevated. *Physics of Metals and Metallography*. 2014. Vol. 115. pp. 809–813.
26. Churyumov A. Y., Kazakova A. A. Prediction of True Stress at Hot Deformation of High Manganese Steel by Artificial Neural Network Modeling. *Materials*. 2023. Vol. 16. No. 1083.
27. Churyumov A. Y., Kazakova A. A., Pozdniakov A. V., Churyumova T. A., Prosviryakov A. S. Investigation of Hot Deformation Behavior and Microstructure Evolution of Lightweight Fe–35Mn–10Al–1C Steel. *Metals*. 2022. Vol. 12. No. 831.